Applied Thermal Engineering 105 (2016) 905–912

Contents lists available at ScienceDirect

Applied Thermal Engineering

journal homepage: www.elsevier.com/locate/apthermeng

Effect of mixture flow stratification on premixed flame structure and emissions under counter-rotating swirl burner configuration

Cheng Tung Chong [a,b,*], Su Shiung Lam [c], Simone Hochgreb [d]

[a] Faculty of Mechanical Engineering, Universiti Teknologi Malaysia, 81310 Skudai, Johor, Malaysia
[b] UTM Centre for Low Carbon Transport in Cooperation with Imperial College London, Universiti Teknologi Malaysia, 81310 Skudai, Johor, Malaysia
[c] Eastern Corridor Renewable Energy Group (ECRE), Environmental Technology Programme, School of Ocean Engineering, University Malaysia Terengganu, 21030 Kuala Terengganu, Terengganu, Malaysia
[d] Department of Engineering, University of Cambridge, Trumpington Street, CB2 1PZ Cambridge, UK

HIGHLIGHTS

- Flame structure of counter swirl flame depends on mixture and flow stratification.
- High swirl flow in the inner annulus generates elongated and enlarged flame reaction zone.
- Mixture and flow stratification affect local emissions.
- Rich stratification of inner channel results in higher NO_x and CO emissions.
- Enrichment of outer annulus shows comparable emission levels to homogenous premixed flames.

ARTICLE INFO

Article history:
Received 25 December 2015
Revised 29 March 2016
Accepted 31 March 2016
Available online 11 April 2016

Keywords:
Counter-rotating
Emissions
Combustor
Swirl flame
OH* chemiluminescence

ABSTRACT

An investigation of the flame structure and emission performance of stratified swirl methane/air flames was performed by using a double-annulus counter-rotating premixed swirl burner. Stratification of the flow and mixtures were established by varying the bulk air flow rates and mixture equivalence ratios between the inner and outer annuli. Two distinct flame fronts were stabilised at the burner outlet, separated by a shear layer due to velocity differences. Higher swirl flow in the inner annulus generates an elongated and enlarged area of flame reaction zone due to increased flame intensity, as the flame shape is strongly dependent on the velocity magnitude exiting the annulus. Mixture and flow stratification affect local emissions. A richer mixture stratification within the inner channel at 70:30 flow split results in 91% and 49% higher emission rates of NO and CO respectively compared to premixed arrangement, in spite generally aiding flame stability. Enrichment of the outer annulus at 70:30 split flow shows only slightly higher levels of NO and CO emissions by 3% and 9% respectively compared to a homogenous mixture.

1. Introduction

Lean premixed swirl-stabilised flame technology is widely employed in many applications such as gas turbines [1], internal combustion engines [2], industrial furnaces [3] and boilers [4] for effective flame and emissions control. Swirl imparts good mixing and stability to flames via the formation of a central recirculation zone which promotes good mixing between incoming reactants and products [5]. Lean premixed flames offer good emissions characteristics, but can become unstable as the temperatures become lower [6]. Additional stability can be obtained at higher equivalence ratios, but at the price of high NO_x emissions. This compromise is often met by using a higher temperature pilot flame. Study of the complexities of swirl within combustors is usually confined to a single annulus swirl configuration [7], while investigation of multiple swirl flames containing a pilot stream is relatively scarce. The establishment of multi-swirl piloted flames results in an equivalence ratio stratification which affects flow field, flame stability, mixing and emissions, which have not been thoroughly characterised.

* Corresponding author at: Faculty of Mechanical Engineering, Universiti Teknologi Malaysia, 81310 Skudai, Johor Darul Ta'zim, Malaysia.
E-mail address: ctchong@mail.fkm.utm.my (C.T. Chong).

http://dx.doi.org/10.1016/j.applthermaleng.2016.03.164
1359-4311/

A few multiple swirl flames established from gaseous and liquid fuels have been studied by Gupta et al. [8] and Durbin and Ballal [9]. Gupta et al. [8] have performed extensive studies on the effect of swirl on flames to show that a double annulus swirl flame burner enables the control of radial distribution of flow and the degree of swirl to achieve stable flames over a wide range of operating conditions. In a related study, Gupta et al. [10] compared the spatial temperature distribution of unconfined double concentric premixed swirl flames under co- and counter-swirl arrangements, showing that the arrangement of the swirl direction, co- or counter-swirl, has great influence on the flame symmetry and stability. In that study, counter-swirl flames were reported to show non-symmetrical temperature fluctuations caused by the thin and intense reaction zone in the flame, which may influence NO_x formation and emissions. Durbin and Ballal [9] concurred with Gupta et al., and observed improved flame stability for flame established from counter-swirl configuration by utilising a double swirl step combustor. The flame length was decreased when the outer vane angle increased and inner air velocity decreased. Lean blow-out was improved when the outer swirl flow intensity was increased. These investigations focused mainly on overall flame structure and stability, but the effect of flow stratification on emissions was not investigated nor quantified.

Liquid fuel injection under multi-swirl configuration has been investigated by some groups. Merkle et al. [11] compared the differences between co- and counter-swirl on the turbulent flow and mixture field of a liquid fuel airblast atomizer. The counter-swirl arrangement was reported to exhibit increased strength of internal recirculation zone as evident by the increased mass flow recirculated but with a reduction of length in axial direction. This is attributed to the faster decay of tangential velocity for counter-rotating air flow, induced by partial compensation of inversely oriented angular momentum fluxes. However, analysis of turbulence quantities show considerable attenuation of the turbulent exchange of momentum perpendicular to the main flow direction for counter-rotating airflows compared to co-rotating flow. This is in contrast to the report by Ateshkadi et al. [12], where counter-swirl configuration increased the radial dispersion of flow for liquid fuel airblast atomizer. The latter further showed that flame stability limits was improved with lower lean blow off limit due to increased strength of recirculation zone, which assists in the transport of fuel droplets.

The performance of emissions using a multiple annulus swirl burner was investigated by Toqan et al. [13]. A radially stratified flame was created via a combination of swirling flow and strong radial density gradient, by injecting fuel through the central nozzle enveloped by rotating air, separating the fuel rich cone from the lean outer region in staged combustion. Low NO_x emissions were achieved through the increased residence time of the mixture under fuel-rich conditions and the use of burned gas recirculation through the burner. Terasaki and Hayashi [14] compared the NO_x emission performance of a double-swirler combustor with the single-swirler of non-premixed, direct central fuel injection burner. The double annulus co-rotating swirl burner was reported to emit low level of NO_x under lean conditions, which was attributed to the rapid mixing process, compared to the conventional swirl burner. To date, there have been no studies on the emissions under counter-swirl double flame configuration.

The present work examines the effect of mixture stratification on the flame structure and emission performance of premixed gaseous flames using a double concentric counter-rotating swirl burner. Quantification of the emissions data and examination of the flame structure provides the insight of the flame shape and stability of a counter-rotating flame burner. The data obtained from the well-defined geometry can also be used as flame modelling validation target.

2. Experimental

2.1. Burner setup and flow delivery system

The schematic of the counter-swirl flame burner and flow delivery system used in the present experiment is shown in Fig. 1a. The swirl flame burner made from stainless steel consists of two annuli with two swirlers placed at the burner outlet. The internal swirler in the inner annulus has eight straight vanes fixed at 45° to the centreline axial axis. The outer swirler comprises of ten straight vanes attached to the swirler hub at 50°. The vane thickness for all vanes (inner and outer swirlers) is 1.5 mm. The internal swirl vanes are arranged in clockwise whereas the outer swirler vanes are arranged in counter-clockwise direction, forming a counter-rotating swirl flow motion at the burner outlet. The pair of swirlers, arranged in concentric at the burner outlet is shown in Fig. 1b. The calculated swirl numbers based on the swirler geometry are $S_N = 0.77$ and 1.04 for the internal and external swirlers respectively, based on the geometric expression

$$S_N = \frac{2}{3}\left[\frac{1-(D_h/D_s)^3}{1-(D_h/D_s)^2}\right]\tan\theta \quad (1)$$

where D_h and D_s represent the swirler hub diameter and the swirler diameter respectively, and θ is the angle of the swirl blade from the centreline [15]. The relatively high swirl number ($S_N > 0.6$) for both swirlers allows the generation of strong swirl with sufficient intensity to stabilise the flame [16]. A circular quartz tube with diameter 100 mm and 150 mm length forms the combustor wall at the burner outlet, allowing optical access for flame visualisation. Table 1 shows the geometry of the double annulus counter-rotating swirl flame burner. For the flow delivery system, four mass flow controllers (Alicat: MCR series, ±1% accuracy full scale) were utilised to supply gaseous fuel (methane) and air to the burner. Methane (99.7% purity, LHV: 50 MJ/kg) was used as the source of hydrocarbon fuel. For each annulus, the air and methane supplies were regulated by mass flow controllers. Premixing of fuel/air for each channel occurs independently at the burner plenum prior to delivery to the burner outlet. The mixtures were ignited at the combustor outlet using a flame torch after both annulus flows were established.

2.2. Operating conditions

The counter-rotating flames were established at different combinations of fuel/air ratios and bulk air flow rates to enable examination of the flame structures and emission performance, as shown in different test series and cases denoted alphanumerically in Table 2. The operating conditions for the investigation of the flame structure via imaging are shown in test series IM, whereas the emissions test operating conditions are shown in the test series of A, B (identical to IM), T, U and V.

These cases are organized as follows: the total air flow rate is always maintained constant, and split between inner and outer annulus, denoted by the air flow split ratio. In case A (baseline), the flame is fully premixed, and the flow rates evenly split, whilst the equivalence ratio is varied. In fully premixed case B (identical to IM), the base flame is kept evenly split at $\phi_{i,o} = 0.7$, while the swirl air split is varied. For case T, the air split ratio and global equivalence ratio are maintained at 50:50 and $\phi_g = 0.8$ respectively, while the equivalence ratio of the annuli are varied from inner to outer enrichment. In case U, the equivalence ratio for the inner and outer annulus are fixed, while the air flow ratio is varied. Finally, for case V, the stratification of the annuli flows is kept fixed, while the air flow split ratio is varied.

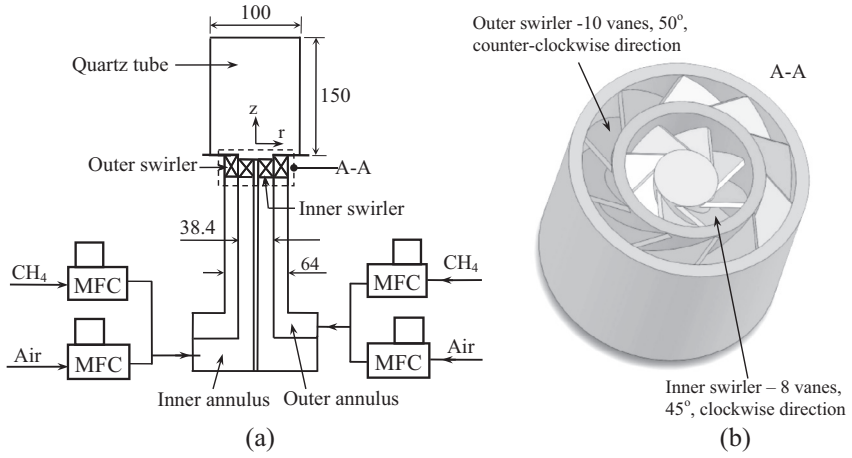

Fig. 1. Schematic of the (a) counter-swirl burner and flow delivery system and (b) swirler set. Dimensions are in millimetres.

Table 1
Geometry of double annulus counter-rotating swirl flame burner.

Inner annulus	
Swirler type	Axial, straight vane
Swirl direction	Clockwise
Swirl number, S_N	0.77
Swirl angle, θ (°)	45
Number of vanes	8
Vane thickness, t (mm)	1.5
Swirl hub diameter, $D_{h,in}$ (mm)	18
Swirler outer diameter, $D_{o,out}$ (mm)	38.4
Effective annulus outlet area, $A_{eff,in}$ (mm^2)	658.8
Blockage ratio	0.43
Outer annulus	
Swirler type	Axial, straight vane
Swirl direction	Counter-clockwise
Swirl number, S_N	1.04
Swirl angle, θ (°)	50
Number of vanes	10
Vane thickness, t (mm)	1.5
Swirl hub diameter, $D_{h,out}$ (mm)	47.0
Burner outlet diameter, $D_{o,out}$ (mm)	64.0
Effective annulus outlet area, $A_{eff,out}$ (mm^2)	1227
Blockage ratio	0.62
Burner wall	
Material	Quartz
Burner outlet diameter, D (mm)	100
Burner wall length, L (mm)	150

Table 2
Operating conditions.

Case	Air split ratio[a]		Inner annulus			Outer annulus				Power (kW)
	Q_i (%)	Q_o (%)	$\dot{m}_{a,i}$ (g/s)	$\dot{m}_{f,i}$ (g/s)	ϕ_i	$\dot{m}_{a,i}$ (g/s)	$\dot{m}_{f,i}$ (g/s)	ϕ_o	ϕ_g	
IM1	30	70	2.38	0.10	0.71	5.55	0.22	0.68	0.70	15.9
IM2	50	50	3.96	0.16	0.71	3.96	0.16	0.68	0.70	16.0
IM3	70	30	5.55	0.23	0.71	2.38	0.09	0.68	0.70	16.2
A1	50	50	3.96	0.16	0.70	3.96	0.16	0.70	0.70	16.2
A2	50	50	3.96	0.17	0.75	3.96	0.17	0.75	0.75	17.3
A3	50	50	3.96	0.18	0.80	3.96	0.18	0.80	0.80	18.5
B1	30	70	2.38	0.09	0.68	5.55	0.23	0.71	0.70	16.1
B2	50	50	3.96	0.15	0.68	3.96	0.16	0.71	0.69	15.9
B3	70	30	5.55	0.22	0.68	2.38	0.10	0.71	0.68	15.7
T1	50	50	3.96	0.15	0.67	3.96	0.21	0.93	0.80	18.5
T2	50	50	3.96	0.21	0.90	3.96	0.16	0.70	0.80	18.5
T3	50	50	3.96	0.22	0.93	3.96	0.15	0.67	0.80	18.5
U1	30	70	2.38	0.09	0.67	5.55	0.27	0.83	0.78	18.0
U2	50	50	3.96	0.15	0.67	3.96	0.19	0.83	0.75	17.3
U3	70	30	5.55	0.22	0.67	2.38	0.11	0.83	0.72	16.6
V1	30	70	2.38	0.11	0.83	5.55	0.22	0.67	0.72	16.6
V2	50	50	3.96	0.19	0.83	3.96	0.15	0.67	0.75	17.3
V3	70	30	5.55	0.27	0.83	2.38	0.09	0.67	0.78	18.0

[a] Total air flow rate is 7.93 g/s and split according to the ratio.

2.3. Measurement techniques

Imaging of the flame reaction zones and global flame structures was performed using an intensified charged-couple device (ICCD) camera (LaVision; IRO Image Intensifier, Imager Pro X 4M). The spectral range of the CCD camera is 290–1100 nm. The camera was coupled with a UV lens fitted with a bandpass filter centred at 308 ± 10 nm to capture the OH* chemiluminescence emitted from the flames. The intensity of OH* chemiluminescence from the flame can be used as an indicator of heat release, where OH* is produced through oxidation of CH before the final steps in the chain at the flame front [17]. However, it must be kept in mind that OH* radiative emission is very dependent on the local equivalence ratio, and thus not a quantitative indicator of reaction rate in partially mixed flames. In the present setup, the gain of the intensifier for OH* chemiluminescence was set to 85% with a gate delay time of 80 μs. A total of 500 images were obtained for each test case.

The post-combustion emissions of NO, NO_2, and CO were measured using a gas analyser (Tocsin 320) at the combustor outlet. The sampling probe was placed 10 mm inward from the combustor outlet to sample across the burner exit plane, at a distance 140 mm from the burner plate. The inlet diameter of the sampling tube is 4 mm and the sampling gas volume is around 6 l/min. The sampling line was heated to the temperature of 180 °C and insulated to prevent condensation of post-combustion products. The spatial emissions values were obtained from 4 equally spaced positions from the burner centreline. The sampling time for each spatial measurement was around 2 min to ensure stabilization of emissions was achieved. The accuracy of the measured NO, NO_2 and CO are 1 ppm, 0.1 ppm and 1 ppm respectively. The gas analyser was calibrated with calibration gases and purged to ensure the readings were zeroed prior to each measurement.

3. Results and discussion

3.1. Global and planar swirl flame structure

The global flame structures derived from line-of-sight OH* chemiluminescence imaging for three different cases of varied

split-air ratio are shown in Fig. 2a–c. The inner and outer equivalence ratios were maintained at $\phi_i = 0.71$ and $\phi_o = 0.68$ respectively, which are close to homogeneous premixed mixture of $\phi = 0.7$, so that the power is approximately constant. The main change in the structures is that the flame length changes with the increasing flow rate of the inner channel flow from case IM1 to IM3. The bulk velocities for the inner annulus are 4.2, 7.0 and 9.8 m/s, and the outer annulus velocities are 5.9, 4.2, 2.5 m/s for case IM1, IM2 and IM3 respectively. The inner and outer flame lengths for IM3 are 40% longer and 60% shorter respectively compared to IM1, roughly in proportion to the bulk velocity changes.

The line-of-sight global OH* chemiluminescence images are Abel transformed to obtain the planar structure of the flames, as shown in Fig. 2d–f. Overall, two different flame fronts are distinguishable, separated by the shear layer between the inner and outer flows. The two flame brushes are in close proximity near the burner outlet and flame root, where the shear is high as a result of the velocity difference between the two swirl flows, enhanced further by the counter-rotating swirl motion. The outer annulus flame is pulled towards the wall, and the flow diverges to partly form a corner recirculation flow while the rest merges with the inner swirl flow to form a centre recirculation flow [18]. The inner swirl flame shows a higher intensity and larger reaction zone, where the main bulk of the heat is released, with highest local temperature [19]. The OH* planar images show that flame shapes are strongly dependent on the magnitude of the velocity from the annulus.

The OH* chemiluminescence intensities for case IM are compared to identify the location of the flame fronts. Fig. 3 shows the half-plane OH* chemiluminescence profiles derived from the axial location of $z/D = 0.31$, 0.44 and 0.58, where z is the axial distance from the burner surface and D is the diameter of the burner outlet. The lower OH* intensity signals for the outer swirl flame fronts relative to the inner swirl flame is due to reduced combustion temperature at leaner conditions [20], as shown in Fig. 3a where the outer swirl flame intensity is approximately lower by a factor of 2 compared to the inner flame. The OH* profiles for case IM2 and IM3 are particularly similar for profiles at $z/D = 0.31$ and 0.44 but slightly different at $z/D = 0.58$ due to the higher inner annulus velocity for the case IM3. However, IM1 shows a slight shift of flame away from the centre. The inner flame is shorter and the outer flame is impinging the wall, as reflected in the OH* intensity plots of Fig. 3b and c. The result shows that IM1 flames are shorter and more compact than IM2 and IM3, indicating that flame shapes and lengths vary depending on the degree of flow stratification.

3.2. Emissions performance

3.2.1. Baselines: Effect of equivalence ratio (case A) and air split ratio (case B)

The baseline emissions for lean premixed homogeneous flames (case A) at an even air split ratio (50:50) are shown in Fig. 4a–c. Overall, the homogeneity of the mixture results in rather flat profiles for NO_2 and CO emissions at the burner outlet for all cases

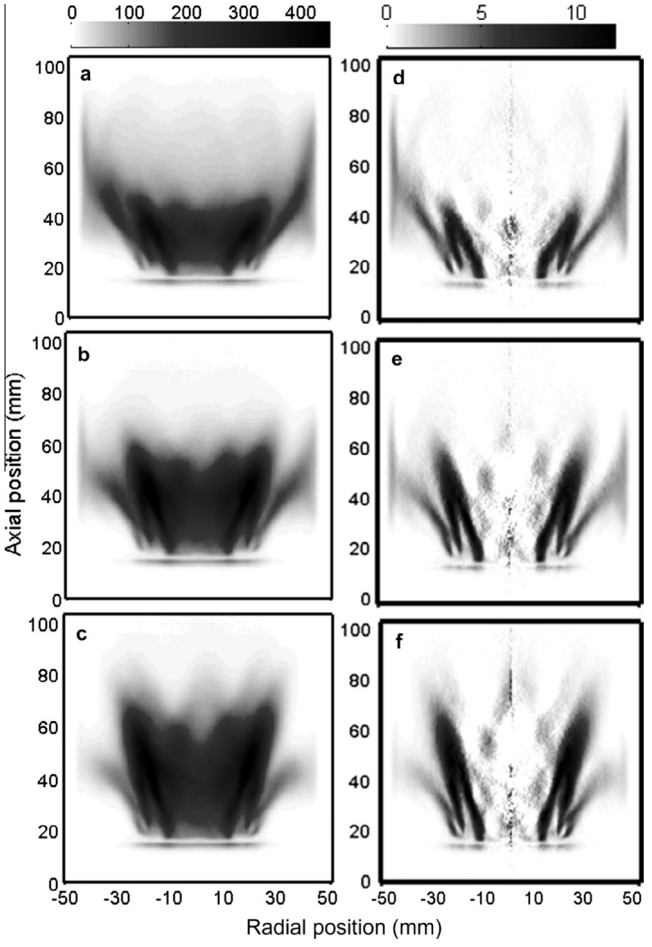

Fig. 2. Global OH* chemiluminescence (a–c) and planar Abel transformed OH* chemiluminescence (d–f) images of counter-rotating flame for air flow split ratio of (a, d) 30:70 (case IM1), (b, e) 50:50 (case IM2) and (c, f) 70:30 (case IM3). The inner and outer equivalence ratios were fixed at $\phi_i = 0.71$ and $\phi_o = 0.68$ respectively.

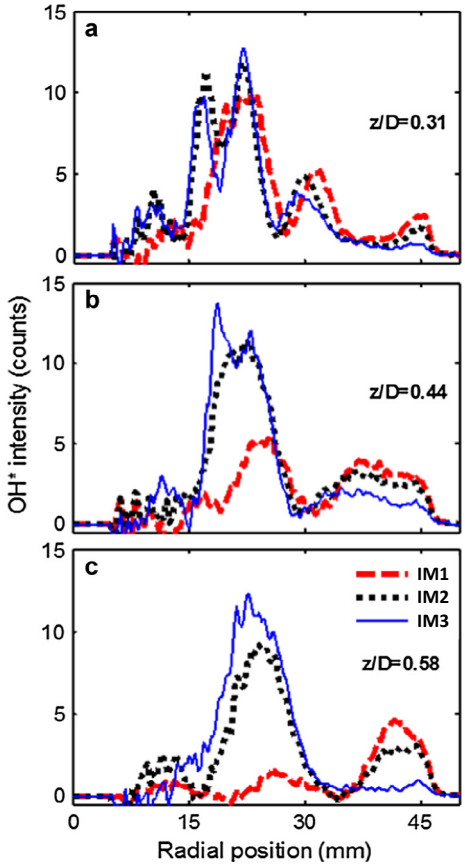

Fig. 3. Half-plane OH* chemiluminescence intensity profiles for IM1, IM2 and IM3 at the axial positions of z/D = (a) 0.31, (b) 0.44 and (c) 0.58 from burner outlet.

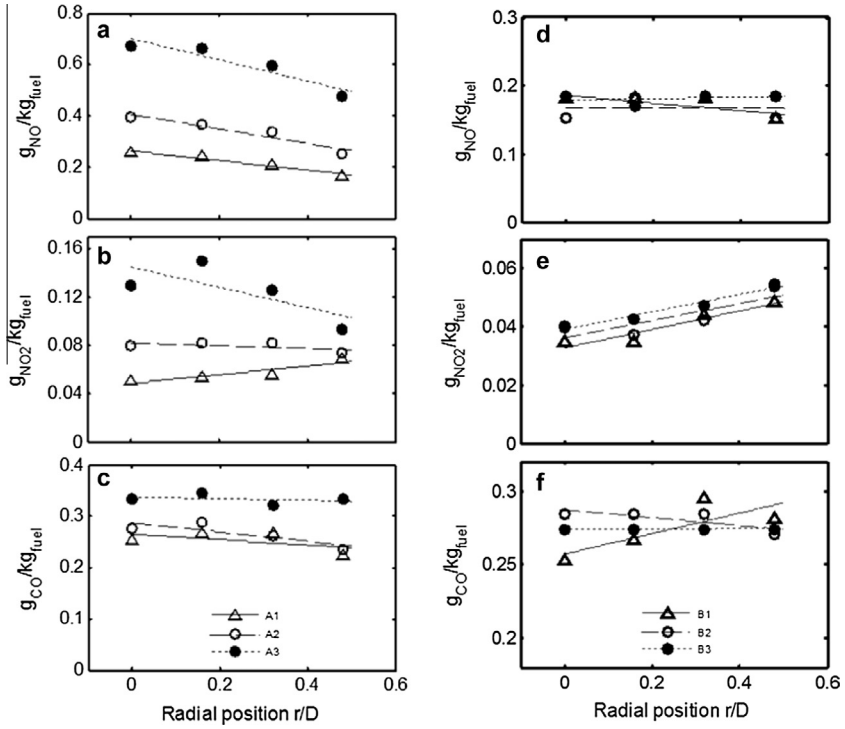

Fig. 4. Emission indices of (a, d) NO, (b, e) NO_2 and (c,f) CO for case A (left column; premixed homogenous flow, even air split flow) and case B (right column; premixed homogenous flow, varied air split flow).

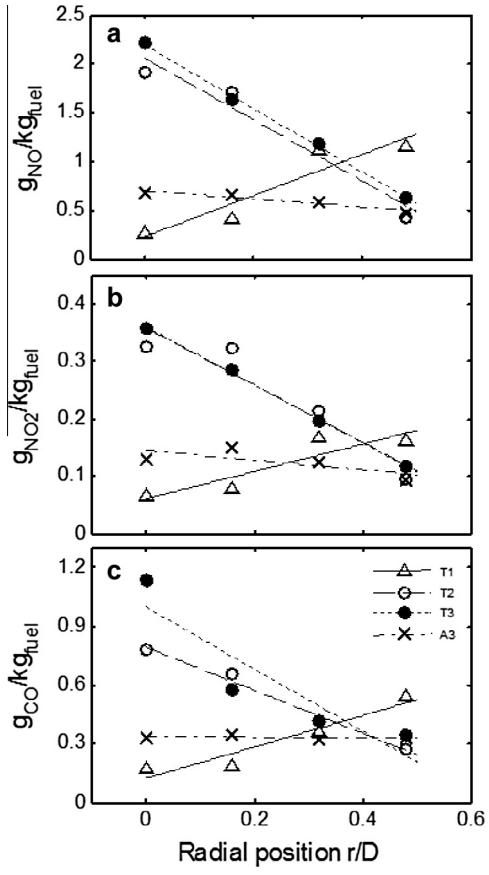

Fig. 5. Emission indices of (a) NO, (b) NO_2 and (c) CO for case T (varied inner and outer ϕ) compared against A3 (homogeneous ϕ for both annuli). The air split ratio is fixed at 50:50.

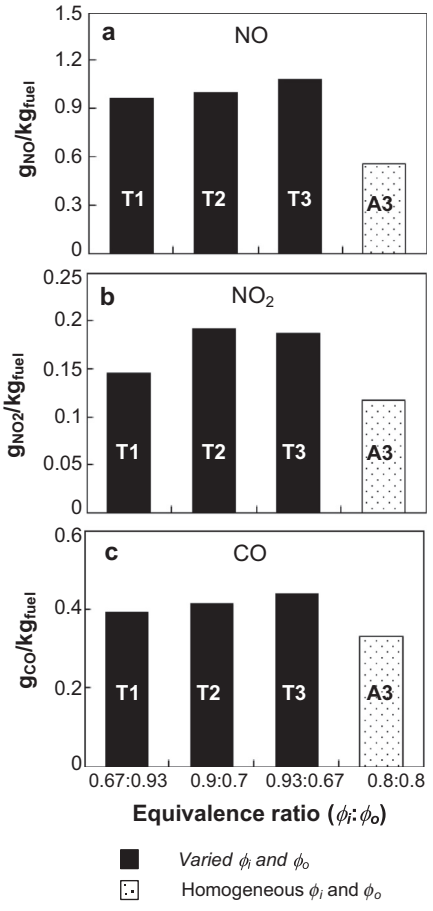

Fig. 6. Area-velocity weighted emission indices of (a) NO, (b) NO_2 and (c) CO for the arrangement of varied lean inner/rich outer (case T) at fixed air split ratio. A3 is set as baseline case. The global equivalence ratios for all cases are $\phi_g = 0.8$.

under fixed counter-rotating swirl flow strength. A slight decreasing trend was observed for NO profile towards the wall region. The increase in emissions of NO and NO_2 is expected with the increase in equivalence ratio due to higher combustion temperature. The smaller increase in CO is, however, unexpected for a premixed flame. In contrast to equivalence ratio, the air split ratio between inner and outer annuli has very little effect on emissions, as shown for premixed case B at $\phi_{i,o} \sim 0.7$ in Fig. 4d–f. This is expected, as the power and equivalence ratio are constant, so that only small details of residence time are changing between cases.

3.2.2. Effect of mixture stratification under fixed air split ratio: Case T

To single out the effect of equivalence ratio, the flow rates for each annulus were fixed at 3.96 g/s while the inner and outer equivalence ratios were varied for case T. The global equivalence ratio for all cases was maintained at $\phi_g = 0.8$ to enable the emission comparison based on the same quantity of fuel injected and constant power output (18.5 kW). Fig. 5a–c shows the emission results of NO, NO_2 and CO compared to the baseline premixed case A3 ($\phi_i = \phi_o = 0.8$) for an even flow rate (air split ratio = 50:50). The higher NO and NO_2 emissions are as expected found in the higher temperature richer regions, in all stratified cases, which track the local equivalence ratio. CO levels also follow the same behaviour found in the premixed cases, with the richer regions producing higher CO levels.

Fig. 6 shows the comparison of overall emission indices for the arrangement of varied inner and outer equivalence ratio (case T) against baseline homogeneous mixture (A3) under the same fixed air split ratio conditions (3.96 g/s for respective annulus). The final emission values were obtained by averaging the spatial emission values across the burner exit and weighted by the area and velocity [21]. The area-velocity weighted values for NO, CO and NO_2 are higher compared to the baseline case, indicating the evident effect of mixture stratification on the emissions. Case T1, the arrangement of inner lean/outer rich configuration, shows the weighted emissions for NO, NO_2 and CO are lower compared to inner rich/outer lean configuration (T2 and T3), but higher than baseline case A3 under identical air split flow. It is also noted that the global equivalence ratio for T1–T3 is the same as A3, where the total fuel flow rate and burner power output is the same. For rich inner/lean outer arrangement (T2, T3), significantly higher NO, NO_2 and CO emissions are shown against baseline A3. The higher emissions for the stratified cases are a result of the highly temperature-dependent NO production rate, so that a non-uniform fuel distribution always result in higher emissions. However, a richer pilot on the inner side consistently leads to higher emissions than a richer outer region because of the longer residence times within the recirculation zones. Conversely, richer pilots produce more stable flames for exactly the same reason.

3.2.3. Effect of air split ratio under fixed stratified mixture: Case U and V

The effect of varied air flow rate split between the two annuli on emissions is investigated for $\phi_i = 0.67$ and $\phi_o = 0.83$. The stratified mixture results in two established flame fronts burning at different temperatures, separated by a shear layer induced by two swirling flows in counter-rotating direction. Fig. 7a–c shows the comparison of the emissions (NO, NO_2 and CO per mass fuel), with case A2 established as the baseline case for reference under homogeneous mixture of $\phi_g = 0.75$ for both inner and outer annuli. All three cases (U1–U3) exhibit lower emissions in the inner region ($r/D = 0$–0.2) where the mixture is leaner, and higher emissions values in the richer regions ($r/D = 0.3$–0.5), as expected from the temperatures produced. A change in the split flow between the two annuli under these conditions does not lead to significant change in NO and NO_2 at the burner outlet. For CO emissions, variation in the inner region is not significant where the mixture is lean, but differences are more evident in the relatively richer outer annulus region. The insensitivity is a result of the fact that the primary factor controlling emissions is temperature, followed by residence times and mixedness between streams.

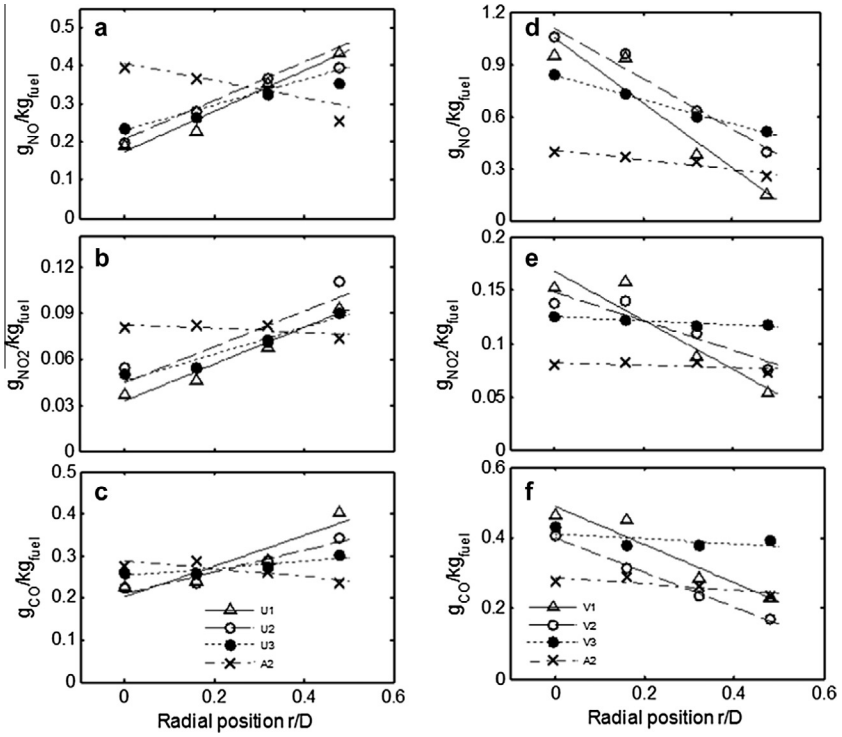

Fig. 7. Emission indices of (a, d) NO, (b, e) NO_2 and (c, f) CO for case U (left column; outer enrichment, varied air split ratio) and case V (right column; inner enrichment, varied air split ratio).

The effect of air split ratio on emissions under stratified mixture conditions (richer inner/leaner outer) is performed by fixing the equivalence ratios of inner and outer annulus at $\phi_i = 0.83$ and $\phi_o = 0.67$ respectively, while varying the air flow rates between the two annuli. Fig. 7d–f shows the emissions of NO, NO_2 and CO for case V compared against the baseline case A2 with a global equivalence ratio $\phi_g = 0.75$. As expected, the result shows higher NO, NO_2 and CO emissions in the richer inner annulus region ($r/D = 0$–0.2) which gradually decrease to lower values in the leaner outer annulus region. The air split ratio does not seem to have an influence. Compared to A2, NO emissions in the outer annulus region for all three cases (V1–V3) are either comparable to or higher than the baseline case, even though mixtures in the outer annulus are much leaner than the inner case. Case V2 and V3 exhibit emission values higher than baseline case at all spatial locations for NO and NO_2. For CO, case V3 shows emission values higher than A2 at all spatial location. The result shows that the emissions are more sensitive to the flow distribution under richer inner/leaner outer arrangement than in the leaner inner/outer richer stratification case. Case V2, in particular, shows higher NO, NO_2 and comparable CO despite having the same air split ratio as baseline case.

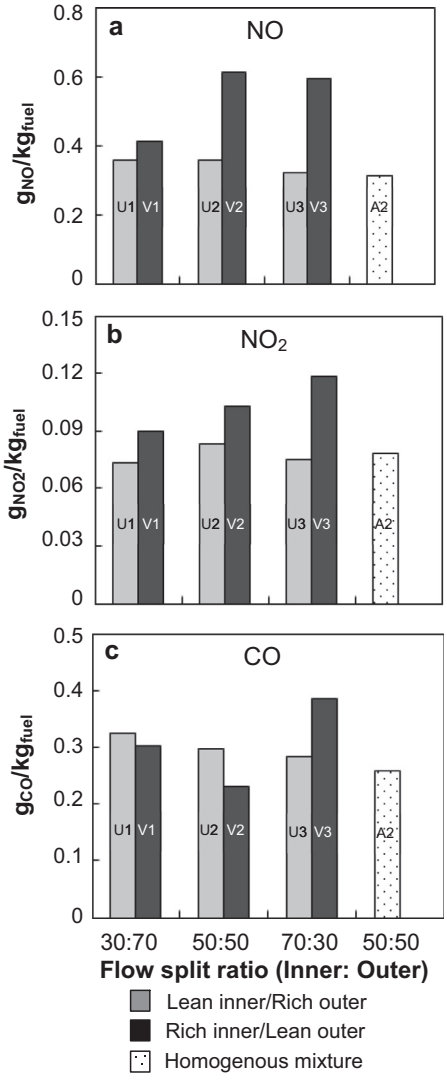

Fig. 8. Area-velocity weighted emission indices of (a) NO, (b) NO_2 and (c) CO for the arrangement of lean inner/rich outer (case U) and rich inner/lean outer (case V). A2 is compared as baseline case.

The establishment of richer inner flames tend to increase local flame temperature that subsequently leads to increased NO production. CO is also evidently higher for case V1 and V3, although V2 did show some slight reduction at the outer annulus region. The incomplete combustion with pockets of unburned fuel contributed by the richer inner flame could be the reason for higher CO formation. For case V1, emissions of NO, NO_2 and CO at $r/D = 0.48$ are consistently lower than baseline. This is due to lower equivalence ratio for V1 at the outer annulus coupled with high flow rate near the wall, which suppresses the mixing of emissions from the inner annulus region.

Fig. 8 shows the overall emission indices for NO, NO_2 and CO as a function of air flow split ratio for the arrangements of lean inner/rich outer (case U) and rich inner/lean outer (case V) annulus. The emissions of homogeneous mixture and even air flow for both inner and outer annuli (case A2) are shown as a baseline reference. The lean inner/rich outer arrangement (case U) produces comparable emission performance ($\sim$0.3 gNO/kg_{fuel}) to the corresponding premixed case A2. The variation of the air flow split ratio affects the total emissions minimally, as the emission is mainly governed by the mixture's equivalence ratio distribution. The inverse arrangement of rich inner/lean outer shows significantly higher NO and NO_2 compared to A2. Case V2 shows higher NO than A2 by a factor of 2. For CO emissions, V1 and V3 show higher values than A2 by 31% and 51% respectively. The high temperature, richer inner annulus region produces high NO, and the lean outer annulus with incomplete combustion produces higher CO.

4. Conclusions

The flame structure and emissions performance of counter-rotating swirl flames under stratified flow and mixture conditions were investigated. Variation of the mixture equivalence ratios and swirl flow between the inner and outer annulus result in distinctly different flame structures, as evident from the global OH^* chemiluminescence imaging. Two swirl flames, independently established by each annulus, were stabilised at the burner outlet and separated by a shear layer. Higher flows in the inner annulus resulted in enlarged main reaction zone with increased flame intensity and thus higher OH^* signals. The flame lengths increase with bulk flow velocities, but the outer flow increase can be smaller, due to impingement of the flame onto the burner wall. Emissions measurements showed the establishment of outer-enriched flames results in only marginally higher levels of NO and CO compared to a baseline homogeneous mixture. Conversely, enrichment of the inner annulus results in significantly higher NO and CO emissions compared to the baseline. This is expected, as a result of the combination of higher temperatures and residence times for inner pilot enrichment. Higher centreline flow rates result in higher emissions for an inner enriched annulus: the longer flame brushes lead to longer exposure to high temperatures, in spite of the higher flow rate. Despite the advantage of enhanced control of flame stability, the emissions performance is in general worse for inner-enriched mixtures, and relatively unchanged for outer enrichment under the same counter-rotating configurations.

Acknowledgements

The financial support from the Ministry of Higher Education Malaysia and Universiti Teknologi Malaysia (Research university grant Tier-1 vot no.: 09H79) and Ministry of Science, Technology and Innovation (MOSTI) Malaysia (project number: 03-01-06-KHAS01) is gratefully acknowledged.

References

[1] C.H. Cho, G.M. Baek, C.H. Sohn, J.H. Cho, H.S. Kim, A numerical approach to reduction of NOx emission from swirl premix burner in a gas turbine combustor, Appl. Therm. Eng. 59 (2013) 454–463.

[2] K. Lee, C. Bae, K. Kang, The effects of tumble and swirl flows on flame propagation in a four-valve SI engine, Appl. Therm. Eng. 27 (2007) 2122–2130.

[3] H. Zhou, R. Tao, Y. Yang, Impact of OFA on combustion and NOx emissions of a large-scale laboratory furnace fired by a heavy-oil swirl burner, Appl. Therm. Eng. 90 (2015) 994–1006.

[4] W.P. Adamczyk, S. Werle, A. Ryfa, Application of the computational method for predicting NOx reduction within large scale coal-fired boiler, Appl. Therm. Eng. 73 (2014) 341–348.

[5] C.T. Chong, S. Hochgreb, Measurements of non-reacting and reacting flow fields of a liquid swirl flame burner, Chin. J. Mech. Eng. 28 (2015) 394–401.

[6] M. Kim, J. Yoon, S. Park, M. Lee, Y. Yoon, Effects of unstable flame structure and recirculation zones in a swirl-stabilized dump combustor, Appl. Therm. Eng 58 (2013) 125–135.

[7] M.F. Mohd Yasin, R.S. Cant, C.T. Chong, S. Hochgreb, Discrete multicomponent model for biodiesel spray combustion simulation, Fuel 126 (2014) 44–54.

[8] A.K. Gupta, M.J. Lewis, S. Qi, Effect of swirl on combustion characteristics of premixed flames, J. Eng. Gas Turbines Power 120 (1998) 488–494.

[9] M.D. Durbin, D.R. Ballal, Studies of lean blowout in a step swirl combustor, J. Eng. Gas Turbines Power 118 (1996) 72–77.

[10] A.K. Gupta, M.J. Lewis, M. Daurer, Swirl effects on combustion characteristics of premixed flames, J. Eng. Gas Turbines Power 123 (2001) 619–626.

[11] K. Merkle, H. Haessler, H. Büchner, N. Zarzalis, Effect of co- and counter-swirl on the isothermal flow- and mixture-field of an airblast atomizer nozzle, Int. J. Heat Fluid Flow 24 (2003) 529–537.

[12] A. Ateshkadi, V.G. McDonell, G.S. Samuelsen, Effect of hardware geometry on gas and drop behavior in a radial mixer spray, Symp. (Int.) Combust. 27 (1998) 1985–1992.

[13] M.A. Toqan, J.M. Beér, P. Jansohn, N. Sun, A. Testa, A. Shihadeh, et al., Low NOx emission from radially stratified natural gas-air turbulent diffusion flames, Symp. (Int.) Combust. 24 (1992) 1391–1397.

[14] T. Terasaki, S. Hayashi, The effects of fuel–air mixing on NOx formation in non-premixed swirl burners, Symp. (Int.) Combust. 26 (1996) 2733–2739.

[15] J.M. Beer, N.A. Chigier, Combustion Aerodynamics, Appl. Sci. Publ., London, 1972.

[16] V. Tangirala, R.H. Chen, J.F. Driscoll, Effect of heat release and swirl on the recirculation within swirl-stabilized flames, Combust. Sci. Technol. 51 (1987) 75–95.

[17] H.N. Najm, P.H. Paul, C.J. Mueller, P.S. Wyckoff, On the adequacy of certain experimental observables as measurements of flame burning rate, Combust. Flame 113 (1998) 312–332.

[18] C.T. Chong, S. Hochgreb, Flow field of a model gas turbine swirl burner, Adv. Mater. Res. 622–623 (2013) 1119–1124.

[19] C.T. Chong, S. Hochgreb, Spray flame study using a model gas turbine burner, Appl Mech. Mater. 316–317 (2013) 17–22.

[20] J.J. Hernandez, M. Lapuerta, J. Barba, Flame stability and OH and CH radical emissions from mixtures of natural gas with biomass gasification gas, Appl. Therm. Eng 55 (2013) 133–139.

[21] H.G. Tao, H.X. Chen, J.L. Xie, Y.P. Hu, An alternative approach to quantifying fluid flow uniformity based on area-weighted average velocity and mass-weighted average velocity, Energy Build. 45 (2012) 116–123.